Graphical Table of Contents

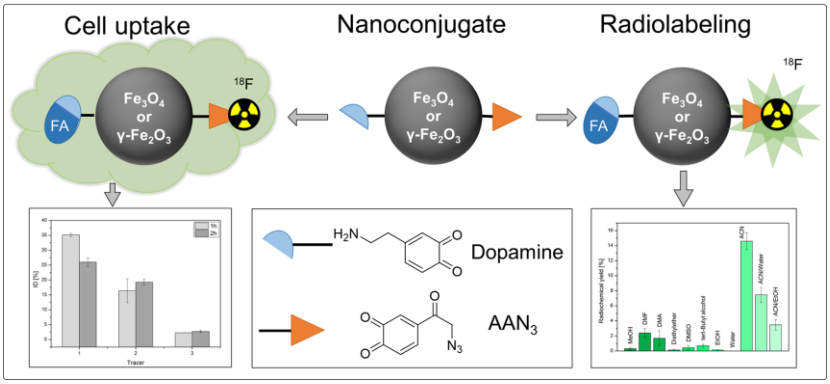

^{18}F-Labeled Magnetic Nanovectors for Bimodal Cellular Imaging

Markus B. Schütz,[a] Alexander M. Renner,[a] Shaista Ilyas,[a] Khan Lê,[a] Mehrab Guliyev,[b] Philipp Krapf,[b] Bernd Neumaier [b] and Sanjay Mathur [a,*]

a. Institute of Inorganic Chemistry, University of Cologne, D-50939 Cologne, Germany.
b. Institute of Neuroscience and Medicine-Nuclear Chemistry (INM-5), Forschungszentrum Jülich, D-52428 Jülich, Germany.

*Correspondence**:** sanjay.mathur@uni-koeln.de Tel: +49 221 470 5627

Abstract

Surface modification of nanocarrier enables selective attachment to specific molecular targets within a complex biological environment. Besides the enhanced uptake due to specific interactions, the surface ligands can be utilized for radiolabeling applications for bimodal imaging ensured by positron emission topography (PET) and magnetic resonance imaging (MRI) functions in one source. Herein, we describe the surface functionalization of magnetite (Fe_3O_4 with folic acid as a target vector. Additionally, the magnetic nanocarriers were conjugated with appropriate ligands for subsequent copper-catalyzed azide-alkyne cycloaddition or carbodiimide coupling reactions to successfully achieve radiolabeling with the PET-emitter ^{18}F. The phase composition (XRD) and size analysis (TEM) confirmed the formation Fe_3O_4 nanoparticles (6.82 nm ± 0.52 nm) The quantification of various surface functionalities was performed by Fourier-transform infrared spectroscopy (FT-IR) and ultraviolet-visible microscopy (UV-Vis). An innovative magnetic-HPLC method was developed in this work for the determination of the radiochemical yield of the ^{18}F-labeled NPs. The as-prepared Fe_3O_4 particles demonstrated high radiochemical yields and showed high cellular uptake in a folate receptor overexpressing MCF-7 cell line, validating bimodal imaging chemical design and magnetic HPLC system. This novel approach, to combine folic acid-capped Fe_3O_4 nanocarriers as a targeting vector with ^{18}F labeling is promising to apply this probe for bimodal PET/MR-studies.

Keywords: magnetic nanoparticles, ^{18}F-labeling, radiolabeled nanoparticles, PET/MR

1. Introduction

Nanoparticles (NPs) of various compositions (e.g. metals, oxides, lanthanide-doped) have gained significant attention in the field of biomedical imaging.[1–10] They are mainly used as contrast agents[11–16] following a significant function in numerous emerging applications such as photodynamic therapy, hyperthermia based cancer treatments or magnetic resonance imaging (MRI).[17] Magnetic NPs are favored as MRI contrast agents[18] due to their low cytotoxicity in the human body as validated by various clinical studies.[19–21] To this end, multimodal imaging and simultaneous therapy can provide complementary information for precise diagnosis and imaging-guided focused tumor therapy, which points out the need for dual-action probes with integrated imaging and therapeutic functions. Positron emission tomography[22–25] (PET) using positron emitters like ^{11}C, ^{13}N, ^{18}F or ^{68}Ga is widely in used in clinical practice for tumor detection or the elucidation of neurological disorders.[23,24,26–33] Fluor-18 is the most frequently applied radionuclide in diagnosis due to its favorable decay properties with a half-life of 109.8 min and low β^+-energy and should also be suited for labeling of NPs.[30,34–41]

The common strategies for producing radioactively labeled nanoparticles include either the labeling of the particle core or of the particle shell. For example, the core of iron oxide nanoparticles can be radioactively labeled by the nuclear reaction $^{58}Fe(n,\gamma)^{59}Fe$, however, due to the natural isotopic distribution of iron (91.72% ^{56}Fe, 2.2% ^{57}Fe and 0.28% ^{58}Fe), the labeling yield is very low, and the irradiation times are very long.[42] A promising alternative involves the co-precipitation of radioactive ^{59}Fe salts for synthesis, where the advantage lies in the high half-life time of ^{59}Fe ($t_{1/2}$ = 45d).[43] A more versatile method is the radioactive labeling of the organic periphery through surface-attached biomolecules, antibodies and other target ligands. *Devaraj et al.* reported on a synthetic route for the radioactive labeling of magnetic iron oxide nanoparticles with [^{18}F]Fluoride in which cross-linked dextran superparamagnetic iron oxide nanoparticles were modified with an ^{18}F-PEG_3 radiotracer.[30] However, the combination of magnetic iron oxide nanoparticles and [^{18}F]Fluoride radiotracer remains elusive due to the orthogonality of functional characteristics and prerequisites of the biomedical imaging protocols.

Folate receptors (glycophosphatidylinositol, FRs) are recognized as a useful therapeutic site due to their overexpression in many tumor sites including lung, colon, breast and ovarian cancers.[44] This membrane protein binds to folic acid with high affinity and facilitates its intracellular transport via endocytic process. Consequently, folic acid has been considered as a potential target ligand for the directed delivery of their payloads to the cancer cells.[44,45] We report here on alkyne-functionalized magnetic nanoparticles for subsequent “click” conjugation[46] for radiolabeling

exhibiting promising labeling yields and site-specific cellular uptake. The carbodiimide coupling reaction was performed on the surface of magnetic carriers to attach folic acid for directing the dual-action labels to the site of interest. In addition, we also report for the first time an innovative purification strategy that efficiently separates nanoparticles from starting materials and unbound radioactive molecules to visualize radioactively labeled particles. The dual-mode labels can be used for magnetic resonance imaging (MRI) and positron emission tomography (PET) studies to demonstrate their potential in selective targeting and bimodal imaging.

Results and Discussion

Magnetite (Fe_3O_4) nanoparticles with different surface functionalities were synthesized by hydrothermal decomposition of an iron (III) salt in the presence of sodium ascorbate as surfactant and reducing agent, 4-(chloroacetyl)catechol (AACl) and dopamine (Fig. 1, step 1). The *in situ* reduction of Fe(III) species (to Fe(II)) was controlled by adding stoichiometric amount of reducing agent. The catechol function of the ligand molecules is essential for the functionalization since it has a strong binding affinity to iron oxides that enabled a stable surface attachment.[47] The folic acid was coupled to the dopamine amino groups exploiting carbodiimide chemistry (Fig. 1, step 3) as targeting molecule for cancer cells with overexpressed folate receptors. The chloride of the AACl was substituted by an azide group (Fig. 1, step 2) for subsequent azide-alkyne cycloaddition reaction. Two different pathways were explored for the radiolabelling. In the first approach, the tosylate (OTs) leaving group needed for subsequent labeling with ^{18}F (Fig. 1, step 5) was conjugated by coupling pent-4-ynyl tosylate to the introduced azide moiety by a copper-catalyzed azide-alkyne cycloaddition (Fig. 1, steps 4 + 5) and the radiolabelling was conducted afterwards. For the other pathway, the radiolabelling building block (^{18}F-pent-4-ynyl) was pre-synthesized separately and then coupled to the azide bound to the nanoparticles (Fig. 1, step 2) using the same copper-catalyzed cycloaddition as before.

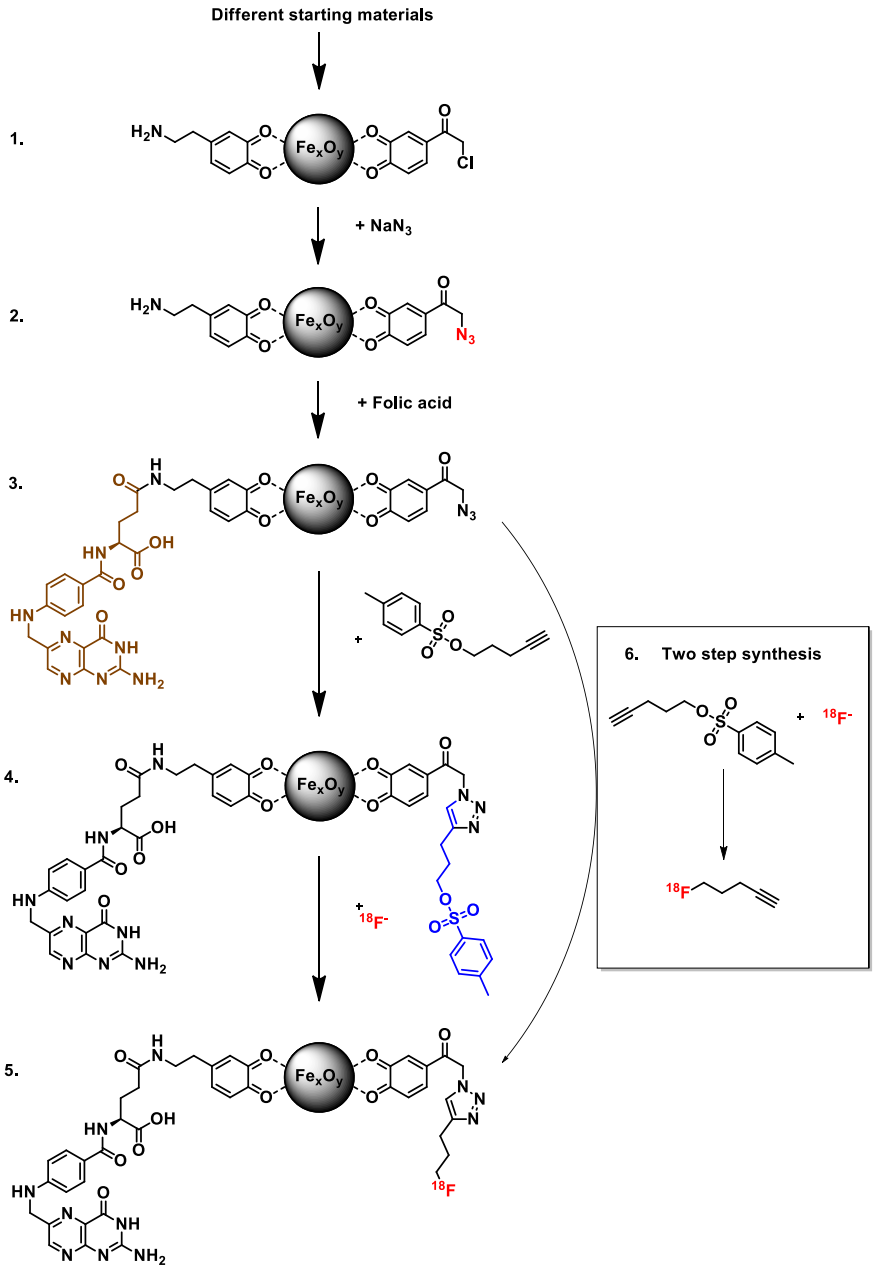

Fig. 1: Reaction scheme for the synthesis and functionalization of Fe_3O_4 nanoparticles following radioactive labeling with ^{18}F by two different reaction pathways. Pathway "1.-5." is a direct labeling approach where the tosylate leaving group is attached to the NPs by the azide-alkyne coupling before ^{18}F labeling. Pathway "1.-3. + 6." Includes the external ^{18}F labeling and subsequent coupling with the labeled building block.

As-obtained nanoparticles displayed spherical shape that was verified by transmission electron microscopy showing an average size of 6.82 nm ± 0.52 nm. The observed agglomeration in the coated iron oxide nanoparticles is possibly due to their ultra-small size and inherent magnetic properties of Fe_3O_4 (Fig. 2 A). The powder X-ray diffraction data confirmed the formation of phase pure Fe_3O_4 particles (Fig. 2 B). The NPs showed enhanced colloidal stability after surface

conjugation with dopamine and 4-(chloroacetyl) catechol ligands displaying an average hydrodynamic radius of 171.10 nm ± 2.51 nm as determined by DLS measurements. The infrared spectra displayed the (Fig. 2 C) vibrational bands corresponding to both surface ligands. The Fe_3O_4 NPs coated with only dopamine possessed a ζ-potential in the positive range (25.90 mV ± 0.25 mV) due to the presence of protonated amino groups on the surface, whereas after modification with AACl, the surface ζ-potential shifted to negative values (-35.2 mV ± 1.01 mV). Consequently, the surface modification of NPs with both dopamine and AACl ligands led to a less negative ζ-potential of -21.35 mV ± 0.29 mV (Fig. 2 E).

The terminal chloride groups of the AAC molecules attached on the surface were replaced by azide groups in a S_N2 nucleophilic substitution reaction. The substitution reaction was confirmed by the observation of the characteristic azide vibration band at a wavenumber 2100 cm^{-1} (Fig. 2 C). Additionally, the ζ-potential change from -21.35 mV ± 0.29 mV to -12.20 mV ± 0.53 mV also suggested a change in the surface chemistry upon individual functionalization steps (Fig. 2 E). The presence of surface-terminating azide groups was necessary to conjugate alkynated-^{18}F for radiolabeling study following Click-chemistry protocol. Furthermore, the amino functionality was used to perform a carbodiimide coupling reaction for the attachment of folic acid that is a UV active targeting ligand. In consequent steps, the NPs were tested for different concentrations of folic acid (0.25 mg/mL, 0.5 mg/mL, 2.5 mg/mL, 5 mg/mL) by performing conjugation reactions under similar reaction conditions. Different amount of folic acid units immobilized on the surface of the nanoparticles was verified by absorption spectra and through the changes in the UV/Vis maxima as a function of the initial quantity of the ligand, as evident in Fig. 2 D. The intensity of λ_{max} in the wavelength range of 272 nm to 282 nm showed a significant decrease depending upon the additional folic acid in the reaction. The ζ-potential changed from -12.20 mV ± 0.53 mV to 32.62 mV ± 0.38 mV indicating a significant alteration on the chemical topography of the particles. The folic acid molecule has several $-NH_2$ groups that can be protonated in aqueous solution that accounts for the significant change in the ζ-potential.

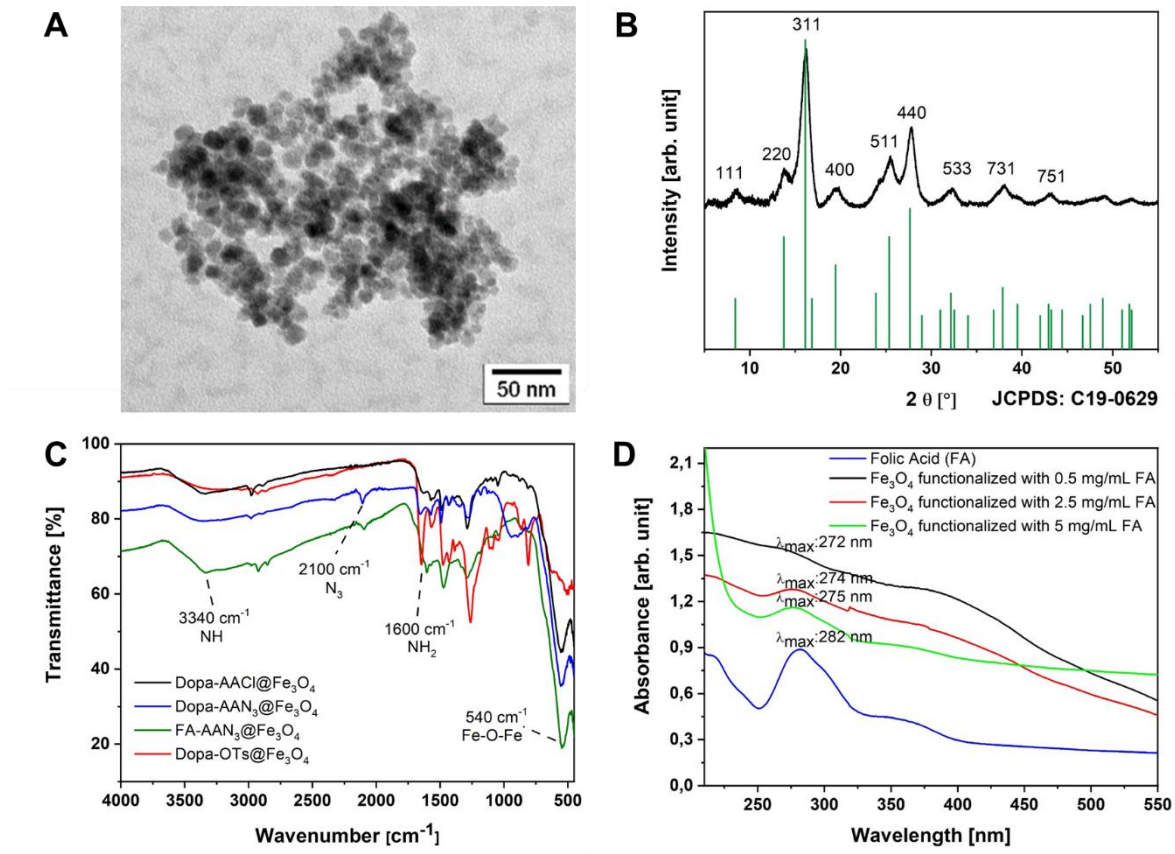

E

Sample	Zeta Value [mV]
$Dopa@Fe_3O_4$	+25.90 ± 0.25
$AACl@+Fe_3O_4$	-35.2 ± 1.01
$Dopa\text{-}AACl@Fe_3O_4$	-21.35 ± 0.29
$Dopa\text{-}AAN_3@Fe_3O_4$	-12.20 ± 0.53
$FA\text{-}AAN_3@Fe_3O_4$	+32.62 ± 0.38
$FA\text{-}OTs@Fe_3O_4$	+20.76 ± 0.57

ς-

Fig. 2: (A) TEM image of the as-synthesized iron oxide NPs with an average size of 6.82 nm.(**B**) XRD pattern of as-synthesized Fe_3O_4 NPs. (**C**) Infrared spectrum of the NPs before and after the functionalization with Dopa and OTs. (**D**) UV-Vis spectra for surface group analysis before and after the functionalization of magnetite NPs with different concentration of folic acid molecule. (**E**) Table containing the potentials values of functionalized NPs. The pH values of particles dispersions were in the range of 5.5 to 6.5.

In order to perform radiolabeling experiments, azide groups of the modified Fe_3O_4 particles were used following two different methods. In the first approach, pent-4-ynyl tosylate (tosylate leaving group)[48] was coupled to the surface of the nanoparticles using the “Click” reaction followed by

direct labeling with the radioactive ^{18}F label. The outcome of the reaction was confirmed by ζ-potential and IR measurements. In the IR spectra, the observable decrease of the azide signal at a wavenumber of 2100 cm^{-1} was visible, indicating the coupling of azide moiety with alkyne groups of pent-4-ynyl tosylate. The specific bands for the triazole group with a wavenumber between 1290 and 825 cm^{-1} could not be clearly detected due to an overlap with other bands in the spectra. The ζ-potential shifted from 32.62 mV ± 0.38 mV to 20.76 mV ± 0.57 mV. The magnitude of the ζ-potential indicated the potential high stability of colloidal nanoconjugates. Additionally, the colloidal stability was characterised and was in a range of 60 min to 420 min. The FA-AAN_3@Fe_3O_4 and AACl@Fe_3O_4 particles showed the highest stability in water.

In the second approach, the magnetic particles were separated from the reaction chamber after the conjugation of ^{18}F labeled pent-4-ynyl tosylate (OTs) followed by the Click reaction. The success of the radiolabeling reaction between azide modified particles and alkynated radioactive ligands was controlled using Radio-HPLC. The results confirmed that after the purification step by distillation only the radioactive product was existent in the reaction chamber that validated the efficacy of magnetic separation approach.

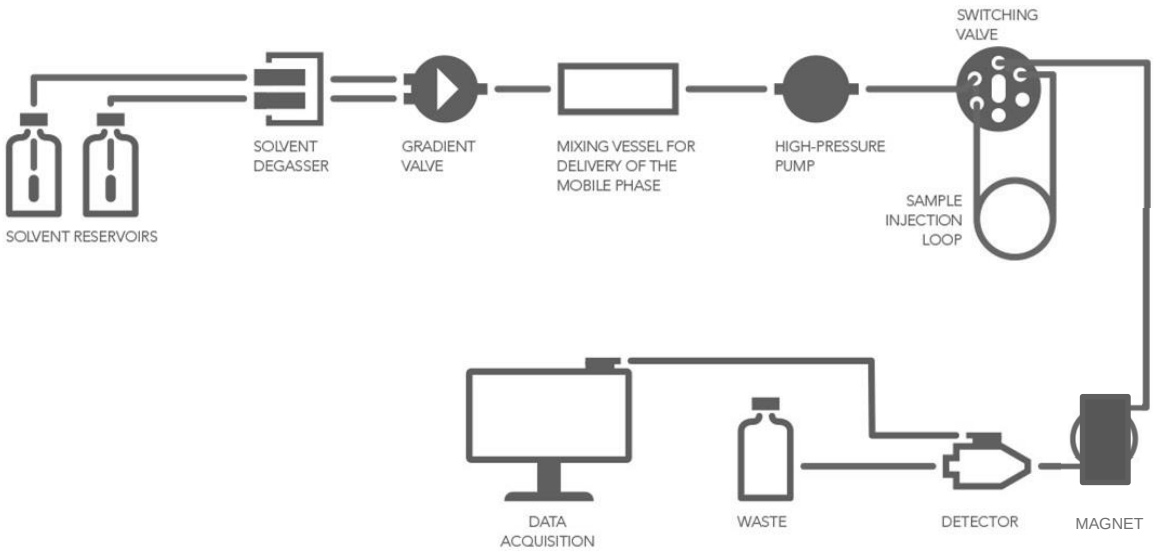

Fig. 3: Schematic construction of the HPLC system with a new component for the separation of magnetic nanoparticles.

In comparison to radioactive labeled proteins or small molecules, nanoparticles have solid surfaces and they tend to agglomerate in different solvents due to interparticular interactions. The appropriate use of a conventional HPLC system with a suitable separation column is not effective because a controlled passage through the column cannot be guaranteed for particle

agglomerates that poses a high risk of blocking the pores of the whole system. Therefore, in this work an innovative set-up was developed for cleaning magnetic nanoparticles, which could be successfully used for radioactive labeled particles as well. For this purpose, instead of the column, a permanent magnet was added to the HPLC system, while the other parts remained the same as shown in Fig. 3. A tube wrapped around the magnet leads to accumulation of the magnetic particles next to the magnet. All nonmagnetic starting materials or side products were washed out continuously. After removing the magnet, the collected magnetic particles were washed out from the tube and detected by a scintillation detector. This cleaning setup was evaluated by two other HPLC systems with different magnetic nanoparticles that confirmed its versatility for the separation of magnetic NPs.

To evaluate the radioactive yield of the folic acid and ^{18}F labeled nanoparticles, different reaction parameters were developed. It was possible to increase the radiochemical yield up to 15% with acetonitrile as solvent during the radioactive labeling. A number of other common solvents that are typically used for nanoparticle dispersions were also analyzed to define the most suitable solvent system. The utilization of MeOH (0.3%), DMF (2.4%), DMA (1.7%), Diethylether (0.13%), DMSO (0.43%), tert-Butyl alcohol (0.7%), EtOH (0.13%), water (0%), ACN/Water (7.47%) and ACN/EtOH (3.47%) led to lower radiochemical yield (Fig. 4).

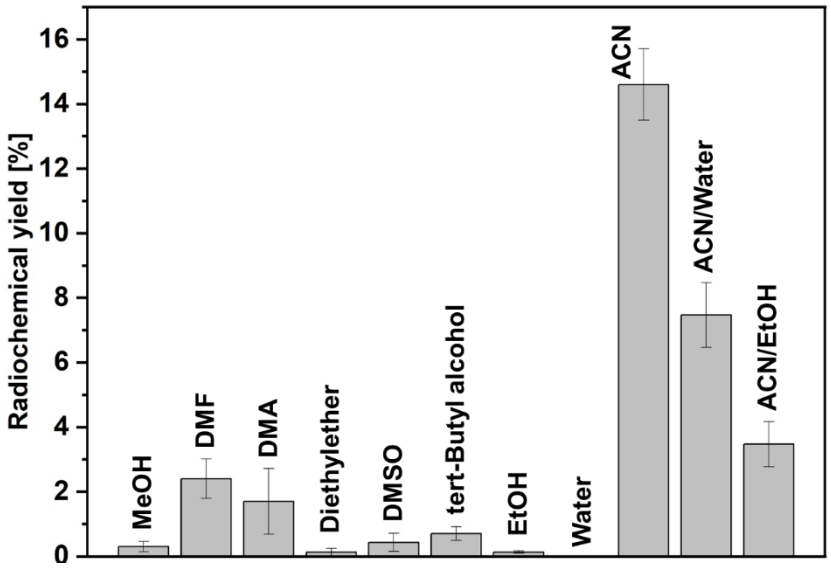

Fig. 4: Graphical evaluation of the radiochemical yield of ^{18}F labeled magnetite NPs in various solvents.

It is necessary to select an appropriate number of input parameters such as reaction temperature and time to evaluate the effectiveness of the labeling yield. The collective assessment of these parameters showed ((Fig. 5) an increase in the labeling efficiency from 0 min to 30 min at a temperature of 80 °C. An increase in the reaction time up to 60 min was found to provide1.09% higher yield. The increase in the temperature from 80 °C to 110 °C did not affect the yield, which shows that surface conjugation is quantitatively achieved already at 80 °C. In conclusion the radioactive labeling gave the best results in acetonitrile at 80 °C with a reaction time of 30 min as shown in Fig. 5.

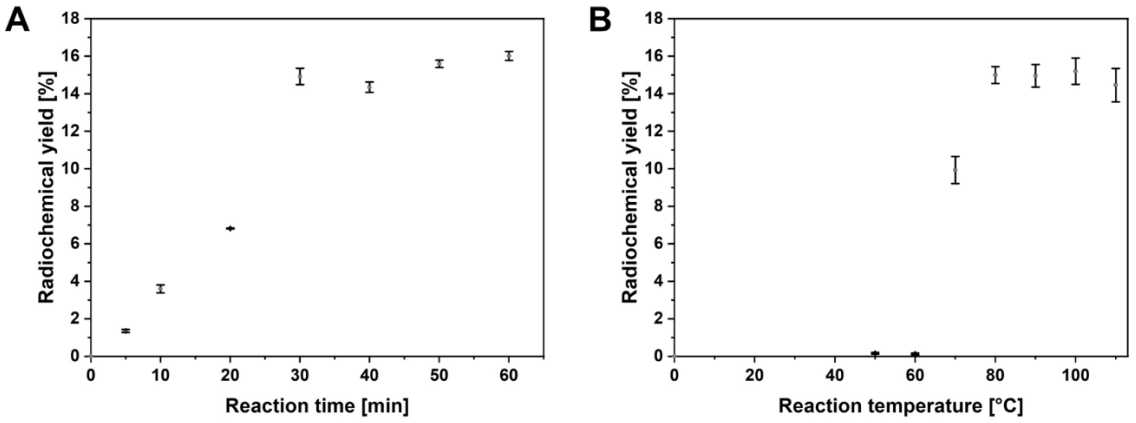

Fig. 5: Optimization of the (A) reaction time and (B) reaction temperature for the radioactive labeling of magnetite nanoparticles with ^{18}F in acetonitrile.

After establishing optimal reaction conditions, the nanoparticles with different concentration of folic acid surface-ligands were labeled in a one-step approach. The particles with the lowest amount of folic acid (0.50 mg/mL) showed the weakest radioactive yield (2.5%) after a reaction at 80 °C for 30 min. The results showed that the radioactive yield increases in relation to the amount of folic acid attached on the surface of the nanoparticles (2.50 mg/mL: 6% RCY, 5.00 mg/mL: 13% RCY). Therefore, the steric hindrance of the folic acid is unlikely to have a significant impact in the examined system, as a reduced amount of folic acid did not increase the radioactive yield.

The one-step labeling offers several benefits in comparison to the multistep labeling approach. Firstly, the RCY is higher (15% compared to 7%) and the overall reaction time is shorter enabling more efficient use of ^{18}F that is a crucial parameter due to the short half-life of the radionuclide.

Secondly, the two-step reaction requires an additional cleaning step after the synthesis of the radiolabeled ligand, resulting in higher losses of particles and the decay of ^{18}F.

The versatility of the surface conjugation and magnetic separation approaches developed in this work was demonstrated for another nanoparticle type by using the same surface chemistry and labeling protocols. The γ-Fe_2O_3 nanoparticles with pronounced magnetic properties and an average size of 250 nm ± 2 nm were synthesized by solution processing to obtain a crystalline material that was confirmed by powder XRD data, which showed the presence of a minor phase that could not be unambiguously detected (Fig. 6 A & B). The particles were tested for a click reaction between 4-(azidoacetyl)catechol and pent-4-ynyl tosylate. After the functionalization, IR-measurement showed the introduced catechol ligand with a stretching frequency at wavenumber 2100 cm^{-1} indicating the presence of the azide function (Fig. 6 C). After the click reaction this vibration band disappeared due to the transformation of the azide moiety into a triazole group. The signals for the catechol ligand in an area between 1500 and 1750 cm^{-1} appeared as somewhat blurred bands. The ζ-potential of the nanoparticles shifted from -11.80 mV ± 0.49 mV to -19.50 mV ± 0.51 mV after functionalization with 4-(azidoacetyl)catechol that changed to -28.30 mV ± 1.76 mV after the completion of Click reaction (Fig. 6 D).

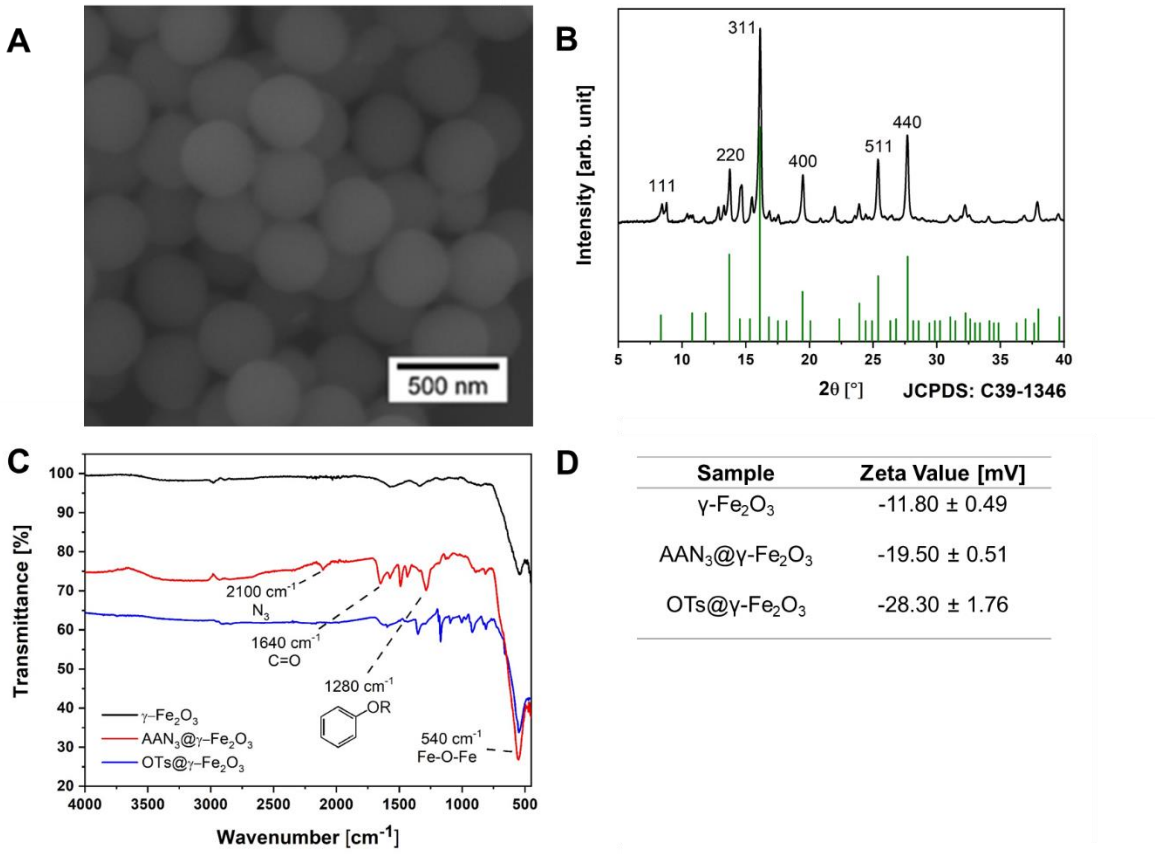

Fig. 6: (A) SEM image of as-synthesized γ-Fe_2O_3 NPs. (B) XRD pattern of as-synthesized Fe_2O_3 NPs. (C) Infrared spectrum of the NPs before and after the functionalization with AAN_3 and OTs. (D) Table containing the **ζ**-potentials of functionalized NPs.

After radiolabeling with ^{18}F under conditions optimized for magnetite particles, the NPs demonstrated a radiochemical yield of 37.79% ± 2.78%. The higher yield in comparison to the folic acid-labeled particles is possibly due the larger size of the particles and the additional higher amount of azide groups on the surface. In comparison, there are no additional extra dopamine groups on the surface which leads to more OTs leaving groups which can react with the free ^{18}F. The attractive labelling yield for these particles shows the practicability of this method that will be useful for nanomedicine and can be adapted for functionalization and radiolabelling of several other magnetic particles with different shapes and surface properties.

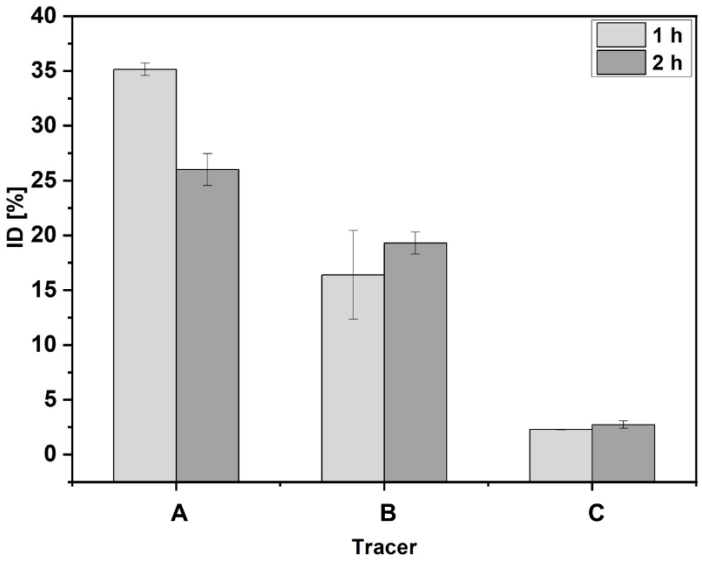

Fig. : Cellular uptake of different radiolabeled materials by MCF-7 cells after 1 and 2 h. The cell concentration was 100 cells per µL. Tracer: (A) [^{18}F]Folic Acid@Fe_3O_4 NPs; (B) [^{18}F]NH_2@Fe_3O_4 NPs; (C) [^{18}F]FET

The cellular uptake of radiolabeled nanoparticles was carried out in triplicates (n = 3) with MCF-7 cancer cells (Fig. 7). The ^{18}F-labeled and folic acid modified Fe_3O_4 nanoparticles showed a 35.15% ± 0.56% efficiency after one hour and a 26.00% ± 1.46% efficiency after two hours of application. For the control sample ^{18}F-labelled Fe_3O_4 nanoparticles without folic acid functionalization were used and a lower uptake (2 h: 19.3% ± 0.99%, 1 h: 16.4% ± 4.03%) was observed. The higher cellular uptake for the folic acid functionalized nanoparticles is possibly due to the overexpression of folate receptors in the MCF-7 cells and is a proof for the successful functionalization.[49] These observations suggest that the cellular uptake of nanoparticles followed a receptor mediated endocytosis.

In comparison to the standard tracer [^{18}F]FET which is used especially for brain tumors, the here described nanoparticle showed a higher cellular uptake as the results known for the standard tracer (2 h: 2.73% ± 0.35%, 1 h: 2.28% ± 0.03%) probes, which are evidently much weaker. This demonstrates the potential of radioactive- labelled nanoparticles for the cellular imaging and can be tested for in vivo cellular imaging of cancer cells.

Conclusions

Hydrothermally synthesized magnetic nanoparticles (Fe_3O_4 and γ-Fe_2O_3) were successfully labelled with ^{18}F-radioactive nuclides and conjugated with folic acid as target ligands following Click chemistry protocols. Precisely, a chemical conjugation approach provided a facile pathway to immobilize tosylate groups on the outer surface of carrier nanoparticles for grafting radiolabeled ligands. The^{18}F-labelled particles were separated and purified in an improved HPLC system developed in this work. Comprehensive characterization of surface-attached functional groups and solution behavior by IR, ζ-potential, and DLS analyses confirmed the presence of amino- and azido-units that could be selectively activated by carbodiimide coupling and cycloaddition reactions to obtain novel dual-action magnetic probes suited for simultaneous MRI and PET imaging. Attachment of different amounts of folic acid units on the surface of nanoparticles by carbodiimide coupling showed that steric hinderance does not play any predominant role in the radiolabeling of nanoparticles and the complementarity of the reaction partners is decisive for obtaining dual-action radioactive magnetic carriers. The challenge of separating the bimodal PET-MRI tracer from the unlabeled nanoparticles and excess ligands was addressed by developing a novel, efficient and economical modification in HPLC set-up that demonstrated the separation efficiency and detection of purified radiolabeled nanoparticles from the starting materials. This component can be useful for differentiation of nanoparticles suspended in various organic solvents for radioactive labeling protocols. The study of radiolabeling efficiency in various solvent systems showed acetonitrile to be most promising with highest radiolabeling yield (>15 %) at 80 °C after 30 min. Additionally, the radioactive and folic acid labeled nanoparticles showed a higher receptor-mediated endocytosis of particles in comparison to the particles without folic acid used as reference. Finally, it was demonstrated, that co-conjugated nanoparticles bearing target ligands and PET source have an extraordinary potential for cellular imaging as compared to standard radiotracers. The results reported here demonstrate the translational potential of magnetic nanocarriers as bimodal tracer systems that can be further improved by attachment of

3. Experimental Section

Instrumentation

Nuclear magnetic resonance (NMR) spectroscopy

^{1}H- and ^{13}C-NMR spectra were recorded at 300 MHz and 75 MHz respectively. The measurements were performed on a *Bruker AV 300 MHz (*Billerica, Massachusetts, USA*)*. The chemical shifts δ are reported in ppm downfield of the internal standard of TMS [δ (^{1}H-NMR) = 0.00 ppm, δ (^{13}C-NMR) = 0.00 ppm]. $CDCl_3$ [δ (1H-NMR) = 7.24 ppm, δ (^{13}C-NMR) = 77.2 ppm] and DMSO-d_6 [δ (^{1}H-NMR) = 2.50 ppm, δ (^{13}C-NMR) = 39.5 ppm] were used as solvents. The coupling constant J is indicated in Hz. The fine structure is designated using the following abbreviations: s (singlet), d (doublet), t (triplet), q (quartet), quin (quintet), sxt (sextet), sep (septet), br (broad) and m (multiplet).

X-ray diffraction (XRD)

XRD measurements were performed on *STOE-STADI MP diffractometer* (*STOE & Cie GmbH,* Darmstadt, Germany) with a Mo-source (Kα = 0.71073 Å). The obtained signals were then compared to JCPDS-data. *WinXPOW (STOE & Cie GmbH,* Darmstadt, Germany*)* was used as software to evaluate the diffractograms.

ζ-Potential & Dynamic light scattering (DLS)

ζ-Potential and DLS measurements were performed on a *Zetasizer Nano ZS* (*Malvern Instruments,* Malvern, UK; λ = 633 nm). Each sample was highly-diluted and dispersed in water. Samples were measured in triplets at 25 °C.

Transmission Electron Microscopy (TEM)

TEM images were taken with a *LEO 912 (Zeiss*, Oberkochen, Germany*)*. A highly-diluted dispersion of each sample in ethanol was prepared. Images were taken after evaporation of the solvent.

UV/Vis-Spectroscopy

The UV/Vis-experiments were performed on a *Lamda 950 (Perkin Elmer,* MA, USA*)* at room temperature. All samples were dissolved or dispersed in water.

Fourier-transform infrared spectroscopy (FTIR)

The IR spectra were recorded by the FT-IR spectrometer *Spotlight 400 FTIR Imaging System* from the company *Perkin Elmer (*MA, USA). All measurements were taken under air conditions on room temperature in a range from 400 to 4000 cm^{-1}. For the graphics the program *Origin* was used.

Scattering electron microscopy (SEM)

All SEM images were recorded by *Nova NanoSEM* from the company *FEI*. For sample preparation the particles were dissolved in ethanol and dried on silicon wafer.

High performance liquid chromatography (HPLC) Analysis

HPLC analysis was carried out using two different systems:
1) *Dionex Ultimate 3000, Thermofisher Scientific* with integrated UV-Detector in combination with a radio detector *HERM LB 500* (high energy radio monitor) (*Berthold Technologies, Bad Wildbach, Germany*).
2) *Knauer pump*, a *Knauer K-2500 UV/VIS detector* (*Knauer*, Berlin, Germany) a manuel *Rheodyne injector* (1 ml loop) and a NaI(Tl) well-type scintillation detector (*EG&G Ortec; modul 276 Photomultiplier Base*) with an *ACE Mate Amplifier* and *BIAS supply* (all from *Ortec Ametek*, Meerbusch, Germany). Data acquisition and interpretation was performed using *Gina software* (*Raytest*).

Chemicals

All reagents and solvents used were obtained from commercial sources (Sigma Aldrich, Alfa Aesar, Fischer Scientific, Carbolution, Linde, Tokyo chemical industry Co. Ltd. and Arcros Organics). The purity of the reagents used was at least 95% and these were used without further purification. All moisture and / or oxygen sensitive reactions were carried out under a nitrogen atmosphere. (4-(Chloroacetyl)catechol – TCI, NaN_3 – Sigma Aldrich, $FeCl_3 \cdot 6\ H_2O$ – Sigma Aldrich, $NaHCO_3$ – Alfa Aesar, Dopamine – Sigma Aldrich, Dicyclohexylcarbodiimid – Sigma Aldrich, *N*-hydroxysuccinimide – Alfa Aesar, Pent-4-ynyl tosylate – Sigma Aldrich, $CuSO_4 \cdot 5\ H_2O$ – Sigma Aldrich)

Methods

Synthesis of Fluor-18

[^{18}F]Fluorid was produced by the ^{18}O(p,n)^{18}F reaction by bombardment of enriched [^{18}O]H_2O with 16.5 MeV protons using a *BC1710 cyclotron* (*The Japan Steel Works Ltd*., Shinagawa, Japan) at the *INM-5* (Forschungszentrum, Jülich).

Synthesis of 4-(azidoacetyl)catechol

500 mg 4-(chloroacetyl)catechol (2.7 mmol, 1 Eq.) was dissolved in 4 mL anhydrous DMF. To this solution, 210 mg NaN_3 (3.23 mmol, 1.2 Eq.) was added and the solution was stirred for 2 h at ambient temperature. Then 10 mL EtOAc was added and the mixture was washed with water three times. The collected organic layer was dried with anhydrous $MgSO_4$. The crude product was washed with a hexane/ether = 5/1 solution and evaporated under vacuum. The white solid was obtained in a yield of 320 mg (62%). The obtained catechol derivative was analyzed by ^{1}H-NMR and IR spectroscopy.

Synthesis of Dopamine+4-(Chloracetyl)catechol (AACl) @ Fe_3O_4 nanoparticles

0.57 g $FeCl_3 \cdot 6\ H_2O$ was dissolved in 10 mL H_2O and stirred for 10 min at ambient temperature. 1.35 g $NaHCO_3$ were dissolved in 10 mL H_2O and added slowly to the iron solution and the solution was stirred 30 min at ambient temperature. Last 0.18 g AACl and 0.19 g Dopamine were dissolved in 10 mL H_2O and added. The solution was stirred for additional 30 min at room temperature. Afterwards the solution was transferred into a Teflon tube and autoclaved at 200 °C for 6 h. The particles were washed several times by centrifugation at 11000 rpm for 30 min and redispersed in H_2O/EtOH. The Fe_3O_4 nanospheres were analysed by XRD, IR, DLS/Zeta measurements and images were recorded with SEM/TEM. The particles were used for surface modification with NaN_3, Folic Acid and Pent-4-ynyl tosylate and subsequently radiolabelled.

Synthesis of PEG-stabilized γ-Fe_2O_3 nanospheres

0.81 g $FeCl_3 \cdot 6\ H_2O$ was mixed with 2.64 g NaAc · 3 H_2O, 1.154 g SDS and 0.4 g PEG 6000 in 24 mL Ethylenglycol. The mixture was transferred into a Teflon tube and autoclaved at 180 °C for 6 h. The particles were washed seven times by centrifugation at 11000 rpm for 30 min and redispersion in H_2O/EtOH. The Fe_3O_4 nanospheres were analysed by XRD, IR, DLS/Zeta measurements and images were recorded with SEM/TEM. The particles were used for surface modification with 4-(azidoacetyl)catechol and subsequent radiolabeling.

Synthesis of 4-(azidoacetyl)catechol@γ-Fe_2O_3 nanospheres

10 mg of Fe_3O_4 nanospheres were dispersed in 5 mL heptane and 100 mg of 4-(azidoacetyl)catechol were added. The mixture was kept in an ultrasonic bath for 30 min and then centrifuged 5 times at 11.000 rpm for 30 min, redispersing the particles in H_2O/EtOH after each centrifugation. The surface modified particles were analyzed by XRD, DLS/Zeta and IR spectroscopy. They were used for radiolabeling.

Synthesis of Dopamine+4-(azidoacetyl)catechol@Fe_3O_4 nanoparticles

10 mg of Dopamine+AACl @ Fe_3O_4 nanoparticles were dispersed in 5 ml anhydrous DMF and 50 mg NaN_3 were added. The mixture was stirred over night at room temperature and then centrifuged 5 times at 11000 rpm for 30 min, redispersing the particles in H_2O/EtOH after each centrifugation.The surface modified particles were analyzed by XRD, DLS/Zeta and IR spectroscopy. They were used for surface modification with Folic Acid and Pent-4-ynyl tosylate and subsequently radiolabelled.

Synthesis of Folic acid+4-(azidoacetyl)catechol@Fe_3O_4 nanoparticles[50]

The Folic acid was attached to the particle surface by carbodiimide coupling. Therefore, folic acid (5-50 mg) was mixed with 24 mg dicyclohexylcarbodiimid (DCC) and dissolved in 5 ml anhydrous DMSO. The mixture was stirred under N_2 atmosphere for 3 h at room temperature. Afterwards 13 mg *N*-hydroxysuccinimide (NHS) were added and the mixture was stirred for 24 h at room temperature. 15 mg of dry dopamine+4-(azidoacetyl)catechol@Fe_3O_4 nanoparticles were dispersed in 5 ml anhydrous DMSO and added to the activated folic acid mixture and stirred at room temperature for another 24 h. The particles were centrifuged 5 times at 11000 rpm for 30 min and redispersed in H_2O/EtOH after each step. In the next steps they were used for surface modification with Pent-4-ynyl tosylate and subsequently radiolabelled. The particles were analyzed by XRD, DLS/Zeta, IR spectroscopy and UV/vis measurement.

Synthesis of Pent-4-ynyl tosylate[51]

To a cooled down solution in an ice bath of TsCl (3.84 g, 20.1 mmol, 1.00 Eq.) in dry pyridine (17ml), 4-Pentyn-1-ol (1.70 g, 20.1 mmol, 1.00 eq.) was added under nitrogen-atmosphere, stirred for 2 h at 0 °C and another 30 min at room temperature. Subsequently 30 ml of dest. H_2O were added to the solution and extracted three times with diethyl ether (30 ml each time). The combined organic layers were dried over $MgSO_4$ and the solvent was removed under reduced pressure. In

a final step, the raw product was purified by column chromatography with a c-Hex/EtOAc-mixture (3:1) to obtain the product as a pale-yellow oil with a yield of 2.24 g (9.40 mmol, 47%). The product was analyzed by NMR spectroscopy and was used for the radiolabeling.

Synthesis of Tosylate@γ-Fe_2O_3 nanospheres

The surface modification with Pent-4-ynyl tosylate was carried out using copper-catalyzed Huisgen cycloaddition. Therefore, stock solutions of $CuSO_4$, L-Histidine and NaAs were prepared to reduce the weighting error. 25 mg $CuSO_4 \cdot 5\ H_2O$ (0.1 mmol), 39 mg L-Histidine (0.25 mmol) and 98 mg NaAs (0.49 mmol) were dissolved in 500 µL H_2O each. 10 mg Pent-4-ynyl tosylate was mixed in this order with 50 µl of the $CuSO_4 \cdot 5\ H_2O$ solution, 5 µL of the L-Histidine solution and 50 µL of the NaAs solution. 10 mg 4-(azidoacetyl)catechol @ γ-Fe_2O_3 nanospheres were dispersed in dest. H_2O and added. The mixture was stirred for 18 h at ambient temperature. The particles were centrifuged 5 times at 11000 rpm for 30 min and redispersed in H_2O/EtOH after each step. In the next step they were used for the radiolabeling with $^{18}F^-$. The particles were analyzed by XRD, DLS/Zeta and IR spectroscopy.

Synthesis of Folic acid+Tosylate@Fe_3O_4 nanoparticles

Similar to the Synthesis of the Tosylate @ γ-Fe_2O_3 nanospheres, the Pent-4-ynyl was attached to the Folic acid+4-(azidoacetyl)catechol @ Fe_3O_4 nanoparticles. 10 mg Pent-4-ynyl tosylate was mixed in this order with 50 µl of the $CuSO_4 \cdot 5\ H_2O$ solution, 50 µL of the L-Histidine solution and 50 µL of the NaAs solution. Folic acid+4-(azidoacetyl)catechol @ Fe_3O_4 nanoparticles were dispersed in dest. H_2O and added. The mixture was stirred for 18 h at ambient temperature. The particles were centrifuged 5 times at 11.000 rpm for 30 min and redispersed in H_2O/EtOH after each step. In the next step they were used for the radiolabeling with $^{18}F^-$. The particles were analyzed by XRD, DLS/Zeta and IR spectroscopy.

Synthesis of Tosylate+Dopamine@Fe_3O_4 nanoparticles

Similar to the synthesis of the Tosylate @ γ-Fe_2O_3 nanospheres and Folic acid+Tosylate @ Fe_3O_4 nanoparticles, the Pent-4-ynyl tosylate was attached to the Dopamine+4-(azidoacetyl)catechol@ Fe_3O_4 nanoparticles. 10 mg Pent-4-ynyl was mixed in this order with 50 µl of the $CuSO_4 \cdot 5\ H_2O$ solution, 50 µL of the L-Histidine solution and 50 µL of the NaAs solution. Dopamine+4-(azidoacetyl)catechol@ Fe_3O_4 nanoparticles were dispersed in dest. H_2O and added. The mixture was stirred for 18 h at ambient temperature. The particles were centrifuged 5 times at 11.000 rpm

for 30 min and redispersed in H_2O/EtOH after each step. In the next step they were used for the radiolabeling with $^{18}F^-$. The particles were analyzed by XRD, DLS/Zeta and IR spectroscopy.

Radiosynthesis

Synthesis of 5-[^{18}F]Fluoro-1-pent-4-ynyl

Aqueous [^{18}F]Fluorid was trapped on a *SepPAK Light Water Accell^{TM} Plus QMA cartridge* (*Waters GmbH*, Eschborn, Germany), washed with methanol (1 ml), and eluted with tetraethylammonium bicarbonate solution (5 mg in 500µl MeOH). Methanol was evaporated under argon stream at 40 °C and 500 mbar within 2-4 min. After cooling to room temperature, the residue was mixed with pent-4-ynyl tosylate (20 µl in 500 µl MeCN). The mixture was stirred for 15 min at 80 °C. The product was purified by distillation at 130°C. The product was analyzed using radio HPLC. HPLC-Conditions: *Chromolith® SpeedROD RP-18 endcapped 50-4.6 HPLC column*; solvent: 0-6 min: 10% MeCN: 90% H_2O; flow rate: 1.5 ml/min, 6-7 min: 80% MeCN: 20% H_2O; flow rate 1,5 ml/min, 7-8 min: 10% MeCN:90% H_2O; flow rate: 1.5 ml/min.

Radiolabeling of Folic acid+4-(azidoacetyl)catechol@Fe_3O_4 NPs with 5-[^{18}F]Fluoro-1-pent-4-ynyl

The synthesized compound 5-[^{18}F]Fluoro-1-pent-4-ynyl was used for the radiolabeling of the nanoparticles. Therefore, a copper-catalyzed Huisgen cycloaddtion was carried out. Stock solutions of $CuSO_4$, L-Histidine and NaAs were prepared to reduce the weighting error. 25 mg $CuSO_4 \cdot 5\ H_2O$ (0.1 mmol), 39 mg L-Histidine (0.25 mmol) and 98 mg Sodium ascorbate (0.49 mmol) were dissolved in 500 µL H_2O each. The purified 5-[^{18}F]Fluoro-1-pent-4-ynyl was mixed with 50 µl of the $CuSO_4 \cdot 5\ H_2O$ solution, 50 µl of the L-Histidine solution and 50 µl of the NaAs solution. 10 mg Folic acid+4-(azidoacetyl)catechol @ Fe_3O_4 nanoparticles were dispersed in 10 ml dest. H_2O and added. The mixture was stirred for different times and different temperatures.

Direct radiolabeling of different nanoparticles

Aqueous [^{18}F]Fluorid was trapped on *a SepPAK Light Water Accell^{TM} Plus QMA cartridge* (*Waters GmBH*, Eschborn, Germany), washed with methanol (1 ml), and eluted with tetraethylammonium bicarbonate solution (5 mg in 500µl MeOH). Methanol was evaporated under argon stream at 40 °C and 500 mbar within 2-4 min. The nanoparticles (Tosylate@γ-Fe_2O_3 nanospheres, Folic acid+Tosylate @ Fe_3O_4 nanoparticles or Tosylate+Dopamine@Fe_3O_4 nanoparticles) were

dispersed in different solvents and directly mixed with the residue. The reaction time and temperature were varied.

Synthesis of [^{18}F]FET

[^{18}F]FET was produced at the cyclotron facility of INM-5 (Forschungszentrum, Jülich) as described previously.[52]

Cell Culture

MCF7 breast tumor cells were obtained from *DSMZ GmbH* (Braunschweig, Germany). MCF-7 cells were cultured in EMEM supplemented with insulin (10 µg/ml), NAA (1%), FBS (10%) and penicillin/streptomycin (1%). The cells were cultured in 75 ml flasks containing 10 ml of the culture medium in a humidified atmosphere of 5% CO_2/ 95% air at 37°C for 4-5 days until they reached 80-90% confluency. Cells were seeded into 12-well plates (10^5 cells/ well containing 1 ml medium) 24 h before the beginning of the cellular uptake experiments.

Cellular Uptake Experiments

[^{18}F]Dopamine@Fe_3O_4 nanoparticles, [^{18}F]Folic acid@Fe_3O_4 nanoparticles and [^{18}F]FET (100-150 kBq/well; 1ml) was added and the cells were incubated at 37°C for 1 and 2 h. Thereafter, the cells were washed two times with medium (1ml), trypsinized, harvested and the accumulated radioactivity was measured in a γ-counter (*Wizard 1470*, PerkinElmer, MA, USA). Each experiment was carried out in triplicate. The cellular uptake of [^{18}F]Dopamine@Fe_3O_4 nanoparticles, [^{18}F]Folic acid@Fe_3O_4 nanoparticles and [^{18}F]FET obtained in experiments performed in parallel were compared using 2-way ANOVA followed by Sidak´s multiple comparison test ($p<0.05$).

Acknowledgement:

The authors would like to acknowledge the financial support and infrastructure provided by the University of Cologne in the frame of the Excellence Strategy and for supporting the UoC-Forum “Transformative Nanocarriers for RNA Transport and Tracking”.

References

[1] L. M. Nieves, J. C. Hsu, K. C. Lau, A. D. A. Maidment, D. P. Cormode, *Nanoscale* **2021**, *13*, 163–174.

[2] S. Ilyas, M. Ilyas, R. van der Hoorn, S. Mathur, *ACS Nano* **2013**, 7, 9655-9663.

[3] B. Klębowski, J. Depciuch, M. Parlińska-Wojtan, J. Baran, *Int. J. Mol. Sci.* **2018**, *19*, 4031.

[4] M. D. Mauricio, S. Guerra-Ojeda, P. Marchio, S. L. Valles, M. Aldasoro, I. Escribano-Lopez, J. R. Herance, M. Rocha, J. M. Vila, V. M. Victor, *Oxid. Med. Cell. Longev.* **2018**, *2018*, 6231482.

[5] A. Jurewicz, S. Ilyas, J. Uppal, I. Ivandic, S. Korsching, S. Mathur, *ACS App. Nano Mater*. **2020,** 3, 1621-1629

[6] L. Labrador-Páez, E. C. Ximendes, P. Rodríguez-Sevilla, D. H. Ortgies, U. Rocha, C. Jacinto, E. Martín Rodríguez, P. Haro-González, D. Jaque, *Nanoscale* **2018**, *10*, 12935–12956.

[7] A. M. Renner, S, Ilyas, K. Wennhold, A. Szymura, S. Roitsch, H. A. Schlößer, S. Mathur, *Langmuir* **2020**, 36, 14819–14828.

[8] M. B. Schütz, S. Ilyas**,** K. Lê, M. Valldor and S. Mathur, *ACS Appl. Nano Mater.* **2020,** 3, 5936–5943

[9] R. Haldavnekar, K. Venkatakrishnan, B. Tan, *Nat. Commun.* **2018**, *9*, 3065.

[10] B. Lin, J. Wu, Y. Wang, S. Sun, Y. Yuan, X. Tao, R. Lv, *Biomater. Sci.* **2021**, *9*, 1000–1007.

[11] S. M. Siribbal, J. Schläfer, S. Ilyas, Z. Hu, K. Uvdal, M. Valldor, S. Mathur, *Cryst. Growth Des.* **2018,** *18*, 633-641

[12] D. P. Cormode, P. C. Naha, Z. A. Fayad, *Contrast Media Mol. Imaging* **2014**, *9*, 37–52.

[13] A. Dash, B. Blasiak, B. Tomanek, A. Banerjee, S. Trudel, P. Latta, F. C. J. M. van Veggel, *ACS Appl. Nano Mater.* **2021**, *4*, 1235–1242.

[14] J. Kim, P. Chhour, J. Hsu, H. I. Litt, V. A. Ferrari, R. Popovtzer, D. P. Cormode, *Bioconjug. Chem.* **2017**, *28*, 1581–1597.

[15] A. L. Bernstein, A. Dhanantwari, M. Jurcova, R. Cheheltani, P. C. Naha, T. Ivanc, E. Shefer, D. P. Cormode, *Sci. Rep.* **2016**, *6*, 26177.

[16] J. Wang, Y. Jia, Q. Wang, Z. Liang, G. Han, Z. Wang, J. Lee, M. Zhao, F. Li, R. Bai, D. Ling, *Adv. Mater.* **2021**, *33*, 2004917.

[17] J. Jeevanandam, A. Barhoum, Y. S. Chan, A. Dufresne, M. K. Danquah, *Beilstein J. Nanotechnol.* **2018**, *9*, 1050–1074.

[18] R. A. Revia, M. Zhang, *Mater. Today* **2016**, *19*, 157–168.

[19] G. Jarockyte, E. Daugelaite, M. Stasys, U. Statkute, V. Poderys, T.-C. Tseng, S.-H. Hsu, V. Karabanovas, R. Rotomskis, *Int. J. Mol. Sci.* **2016**, *17*, 1193.

[20] Q. Feng, Y. Liu, J. Huang, K. Chen, J. Huang, K. Xiao, *Sci. Rep.* **2018**, *8*, 2082.

[21] M. A. Abakumov, A. S. Semkina, A. S. Skorikov, D. A. Vishnevskiy, A. V Ivanova, E. Mironova, G. A. Davydova, A. G. Majouga, V. P. Chekhonin, *J. Biochem. Mol. Toxicol.* **2018**, *32*, e22225.

[22] S. Berke, A.-L. Kampmann, M. Wuest, J. J. Bailey, B. Glowacki, F. Wuest, K. Jurkschat, R. Weberskirch, R. Schirrmacher, *Bioconjug. Chem.* **2018**, *29*, 89–95.

[23] B. D. Zlatopolskiy, J. Zischler, D. Schäfer, E. A. Urusova, M. Guliyev, O. Bannykh, H. Endepols, B. Neumaier, *J. Med. Chem.* **2018**, *61*, 189–206.

[24] L. Feni, M. A. Omrane, M. Fischer, B. D. Zlatopolskiy, B. Neumaier, I. Neundorf, *Pharmaceuticals* **2017**, *10*, 99.

[25] E. J. Keliher, T. Reiner, G. M. Thurber, R. Upadhyay, R. Weissleder, *ChemistryOpen* **2012**, *1*, 177–183.

[26] A. R. Jalilian, J. Osso Jr, *Iran. J. Nucl. Med.* **2017**, *25*, 1–10.

[27] C. J. Anderson, R. Ferdani, *Cancer Biother. Radiopharm.* **2009**, *24*, 379–393.

[28] A. Sasikumar, A. Joy, M. R. A. Pillai, B. S, S. SR, *Clin. Nucl. Med.* **2017**, *42*.

[29] E. A. Aalbersberg, B. J. de Wit – van der Veen, M. W. J. Versleijen, L. J. Saveur, G. D. Valk, M. E. T. Tesselaar, M. P. M. Stokkel, *Eur. J. Nucl. Med. Mol. Imaging* **2019**, *46*, 696–703.

[30] N. K. Devaraj, E. J. Keliher, G. M. Thurber, M. Nahrendorf, R. Weissleder, *Bioconjug. Chem.* **2009**, *20*, 397–401.

[31] L.-L. Zhang, W.-C. Li, Z. Xu, N. Jiang, S.-M. Zang, L.-W. Xu, W.-B. Huang, F. Wang, H.-B. Sun, *Eur. J. Nucl. Med. Mol. Imaging* **2021**, *48*, 483–492.

[32] R. J. Hicks, P. Jackson, G. Kong, R. E. Ware, M. S. Hofman, D. A. Pattison, T. Akhurst, E. Drummond, P. Roselt, J. Callahan, R. Price, C. Jeffery, E. Hong, W. Noonan, A. Herschtal, L. J. Hicks, M. Harris, A. Hedt, B. M. Paterson, P. Donnelly, *J. Nucl. Med.* **2018**, jnumed.118.217745.

[33] H. D. Zacho, R. F. Fonager, J. B. Nielsen, C. Haarmark, H. W. Hendel, M. B. Johansen, J. C. Mortensen, L. J. Petersen, *J. Nucl. Med.* **2020**, *61*, 344–349.

[34] C. Bouter, Y. Bouter, *Front. Med.* **2019**, *6*, 71.

[35] P. K. Garg, S. J. Lokitz, L. Truong, B. Putegnat, C. Reynolds, L. Rodriguez, R. Nazih, J. Nedrelow, M. de la Guardia, J. K. Uffman, S. Garg, P. S. Thornton, *PLoS One* **2017**, *12*, e0186340.

[36] J. W. Kiser, J. R. Crowley, D. A. Wyatt, R. K. Lattanze, *Front. Med.* **2018**, *5*, 143.

[37] G. Luurtsema, H. H. Boersma, M. Schepers, A. M. T. de Vries, B. Maas, R. Zijlma, E. F. J. de Vries, P. H. Elsinga, *EJNMMI Radiopharm. Chem.* **2016**, *1*, 7.

[38] M. Pretze, C. Wängler, B. Wängler, *Biomed Res. Int.* **2014**, *2014*, 674063.

[39] T. H. Ribeiro, R. S. Filho, A. C. G. Castro, E. Paulino, M. Mamede, *Rev. Assoc. Med. Bras.* **2017**, *63*, 109–111.

[40] Z. Sun, K. Cheng, F. Wu, H. Liu, X. Ma, X. Su, Y. Liu, L. Xia, Z. Cheng, *Nanoscale* **2016**, *8*, 19644–19653.

[41] M. Takeuchi, T. Nihashi, A. Gafter-Gvili, F. J. García-Gómez, E. Andres, D. Blockmans, M. Iwata, T. Terasawa, *Medicine (Baltimore).* **2018**, *97*.

[42] M.-T. Zhu, W.-Y. Feng, Y. Wang, B. Wang, M. Wang, H. Ouyang, Y.-L. Zhao, Z.-F. Chai, *Toxicol. Sci.* **2009**, *107*, 342–351.

[43] R. Weissleder, D. D. Stark, B. L. Engelstad, B. R. Bacon, C. C. Compton, D. L. White, P. Jacobs, J. Lewis, *Am. J. Roentgenol.* **1989**, *152*, 167–173.

[44] S. Ilyas, N. K. Ullah, M. Ilyas, K. Wennhold, M. Iqbal, H. A. Schlößer, M. S. Hussain, S. Mathur, *ACS Biomater. Sci. Eng.* **2020**, 6, 6138–6147

[45] L. Wortmann, S. Ilyas, D. Niznansky, M. Valldor, K. Arroub, N. Berger, K. R, J. Holmes, and S. Mathur, *ACS Appl. Mater. Interfaces* **2014**, 6, 16631–16642

[46] A. Szymura, S. Ilyas, M. Horn, I. Neundorf, S. Mathur, *Journal of Molecular Liquid, J. Mol. Liq.* **2020**, 317, 114002

[47] K. V Korpany, D. D. Majewski, C. T. Chiu, S. N. Cross, A. S. Blum, *Langmuir* **2017**, *33*, 3000–3013.

[48] M. Pretze, D. Pietzsch, C. Mamat, *Molecules* **2013**, *18*, 8618–8665.

[49] J. P. Marshalek, P. S. Sheeran, P. Ingram, P. A. Dayton, R. S. Witte, T. O. Matsunaga, *J. Control. Release* **2016**, *243*, 69–77.

[50] P. Patra, S. Mitra, N. Debnath, P. Pramanik, A. Goswami, *Bull. Mater. Sci.* **2014**, *37*, 199–206.

[51] A. M. Klester, C. Ganter, *Helv. Chim. Acta* **1983**, *66*, 1200–1209.

[52] K. Hamacher, H. H. Coenen, *Appl. Radiat. Isot.* **2002**, *57*, 853–856.

Supporting Information

^{18}F Labeled Magnetic Nanovectors for Bimodal Cellular Imaging

Markus B. Schütz,[a] Alexander M. Renner,[a] Shaista Ilyas,[a] Khan Lê,[a] Mehrab Guliyev,[b] Philipp Krapf,[b] Bernd Neumaier [b] and Sanjay Mathur [a, *]

a. Institute of Inorganic Chemistry, University of Cologne, D-50939 Cologne, Germany.
b. Institute of Neuroscience and Medicine-Nuclear Chemistry (INM-5), Forschungszentrum Jülich, D-52428 Jülich, Germany.

[*]Correspondence**:** sanjay.mathur@uni-koeln.de Tel: +49 221 470 5627

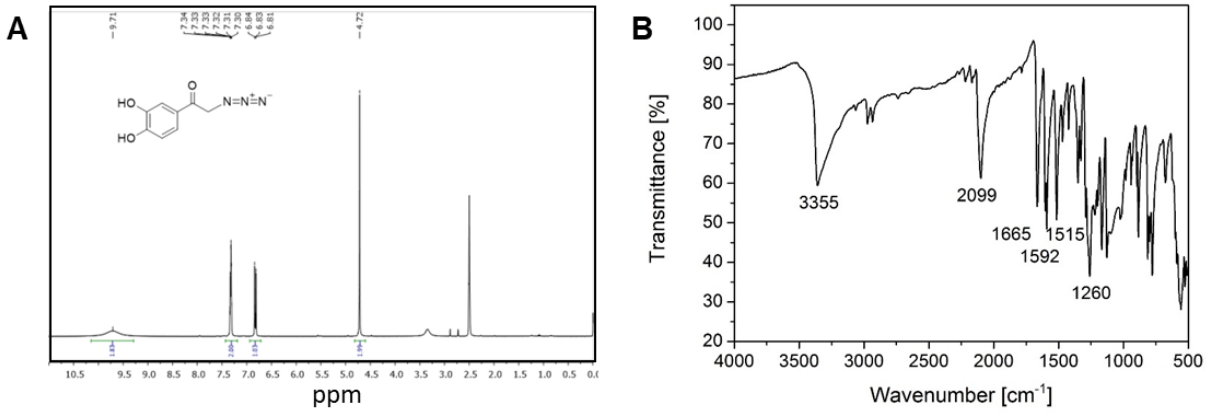

Fig. SI1: (A) ^{1}H-NMR and (B) IR spectrum of 4-(azidoacetylcatechol).